Lift Coefficient Measurement: Experimental Results

April 23, 2025

ME 207: Fluid Dynamics

Project 12

Lift measurement for external flow over aircraft wing

Group 7

Anuj Manoj Joshi	23110033
Jatin Agarwal	23110147
Tanushka Anand Sonde	23110332
Vardayini Agrawal	23110353
Yug Mitulkumar Desai	23110370

Contents:

Objective: 3

Theoretical Discussion and Background: 3

Experimental Setup 6

Measurements: 12

Results and Analysis: 13

Uncertainty Analysis: 24

References 29

Conclusion 29

Acknowledgement 30

Objective

This experiment's primary objective is to investigate an airfoil's lift characteristics under varying flow conditions. Specifically, the experiment aims to:

1. Measure the lift force on an airfoil at different angles of attack and freestream velocities (corresponding to different Reynolds numbers).
2. Determine the lift coefficient (C_L) for each test condition and observe its variation with respect to the angle Angletack and the Reynolds number.
3. Compare the experimentally obtained lift coefficients with theoretical or computational predictions, evaluating deviations and underlying causes.
4. Quantify experimental errors and uncertainties in all measured parameters, including lift force, velocity, and an Angle of attack, to assess the reliability and accuracy of the results.

Theoretical Discussion and Background

The generation of lift on an airfoil is a fundamental concept in aerodynamics, resulting from the interaction between the airfoil surface and the surrounding airflow. It arises mainly due to the pressure difference between the upper and lower surfaces of the wing, and to a smaller extent from the shear (friction) forces along the surface.

When air flows over a wing-shaped body, it moves faster over the curved upper surface and slower underneath. This difference creates lower pressure on the top and higher pressure underneath, resulting in a net upward force. The components of the pressure and wall shear forces in the direction normal to the flow tend to move the body in that direction, and their sum is called lift.

1. Lift Force and Lift Coefficient

The lift force L acting on an airfoil can be expressed as:

$$L = C_L \cdot \frac{1}{2}\rho V^2 A$$

- L: Lift force (N)
- C_L: Lift coefficient (dimensionless)
- ρ: Density of air (kg/m^3)
- V: Freestream velocity (m/s)
- A: Planform area of the airfoil (m^2)

The lift coefficient C_L is a non-dimensional parameter quantifying the lift produced relative to the dynamic pressure and area. It depends on the angle of attack, Reynolds number, and airfoil geometry.

2. Angle of Attack and Thin Airfoil Theory

For a symmetric thin airfoil in inviscid, incompressible flow, Thin Airfoil Theory provides a linear relationship between lift coefficient and angle attack α (in radians):

$$C_L = 2\pi\alpha$$

This relation holds well for small angles of attack (typically less than 10°) and under ideal flow conditions. As α increases, C_L increases linearly until the stall point.

Beyond a critical angle of attack, flow separation occurs over the upper surface of the Airfoil, leading to a sudden drop in lift—a phenomenon known as stall.

3. Reynolds Number and Flow Regimes

The Reynolds number Re is a dimensionless quantity used to predict flow patterns in different fluid flow situations. It is given by:

$$Re = \frac{\rho V L}{\mu}$$

- L: Length (Here chord length of the Airfoil (m))
- μ: Dynamic viscosity of air (Pa·s)

The Reynolds number influences the nature of the boundary layer (laminar or turbulent), which in turn affects the lift and drag characteristics. Higher Re generally results in thinner boundary layers, delayed flow separation, and improved lift performance.

4. Lift Force from Pressure Distribution

When detailed pressure measurements are available over the surface of a wing, the lift force can be determined by integrating the pressure and shear stress contributions:

$$dF_L = -P \sin\theta \, dA + \tau_w \cos\theta \, dA$$

Where:

- P = Local pressure on the surface
- τ_w = Wall shear stress
- θ = An angle between the local surface normal and the freestream direction
- dA = Differential surface area

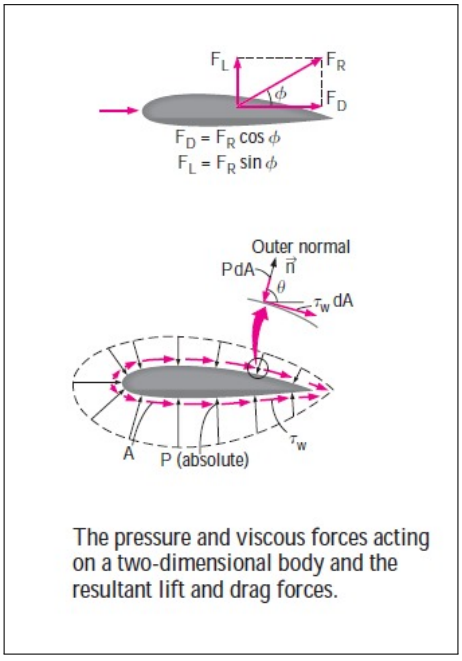

The pressure and viscous forces acting on a two-dimensional body and the resultant lift and drag forces.

By integrating over the entire surface of the wing:

$$F_L = \int_A (-P \sin\theta + \tau_w \cos\theta) \, dA$$

In many practical cases, especially at low angles of attack and moderate Reynolds numbers numbers, the shear contribution is small, and the lift force is dominated by the pressure difference between the top and bottom surfaces.

In real experimental conditions, several factors can cause deviations from ideal theoretical predictions:

- Viscous effects lead to boundary layer development, flow separation, and wake formation.
- Three-dimensional effects (especially in finite wings) introduce induced drag and modify lift distribution.
- Wind tunnel wall interference, surface roughness, and instrumentation limitations contribute to measurement errors.

Thus, experimental results are often compared with theoretical curves, and error analysis is essential for interpreting the accuracy of findings.

Note: We have used a different method to calculate the Lift Force since we don't know the shear stress τ_w

Experimental Setup:

To investigate the lift generated by an airfoil, we devised an experimental setup *aimed at determining* the pressure distribution over the wing surface. By measuring the gauge pressure at multiple points above and below the Airfoil, we aimed to quantify the pressure differential responsible for lift. This setup enabled us to evaluate the aerodynamic behaviour of the Airfoil under controlled wind tunnel conditions.

- **Airfoil Model and Mounting Mechanism:**
  - NACA 4412 airfoil was fabricated using 3D printing for aerodynamic testing.
  - The airfoil surface was embedded with 20 pressure tap holes:
    - 10 on the upper surface
    - 10 on the lower surface
  - The Airfoil was hollow and open from both ends, allowing easy access to the internal pressure tubes from either side.
  - The Airfoil was mounted onto a custom-designed 3-D printed stand, which slides into a socket at the base of the Airfoil for secure fitting.
  - This stand was clamped to the entrance of the wind tunnel to ensure stability during the experiment and to *ensure* that the Airfoil was properly aligned to face the oncoming airflow.

– The base of the stand featured a rotational mechanism, allowing it to rotate even after being clamped, enabling adjustable control over the angle of attack (Aoa).

– To prevent wobbling of the Airfoil at higher wind speeds, a string was passed through the Airfoil from one side to the other, and its ends were tied to the wind tunnel walls for lateral stabilization.

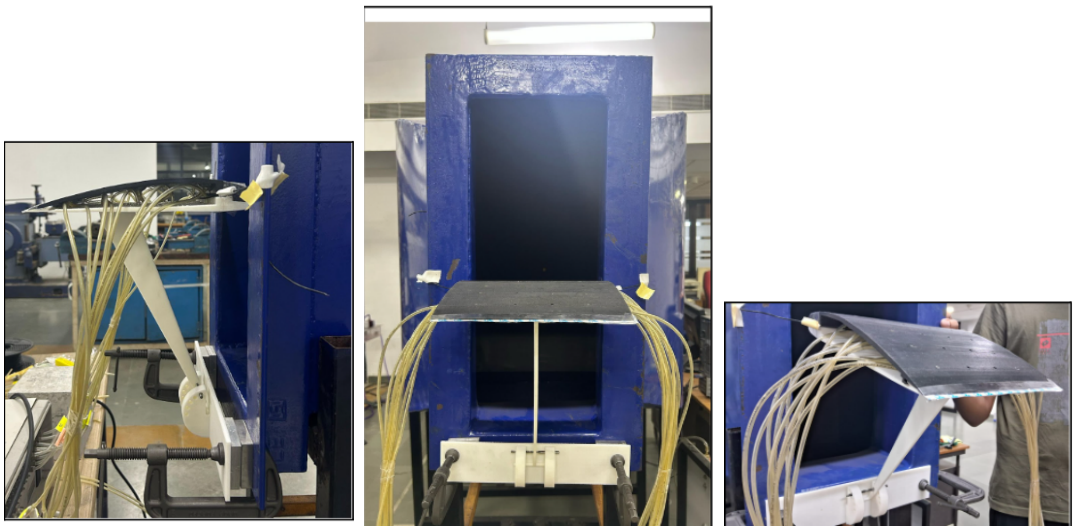

Images of the airfoil model with the mount

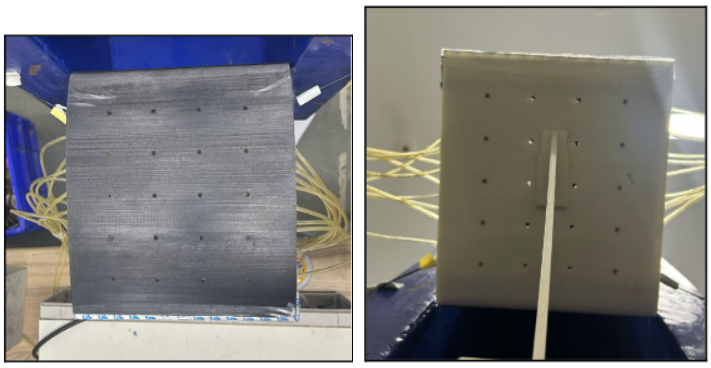

Images of the pressure taps created on the top and bottom surfaces of the Airfoil

- **Pressure Measurement System:** Pressure Scanner and Digital Manometer
  - A pressure scanner and a digital manometer were used to measure the gauge pressure at various pressure taps embedded in the Airfoil.
  - Flexible pressure tubes were *properly labelled* and inserted into the respective holes on the airfoil surface:
    * Care was taken to ensure that the tubes fit securely without protruding from the surface, *so as not* to disrupt the pressure reading or airflow.
    * Tubes were routed carefully to avoid interfering with the airflow, particularly beneath the lower surface of the Airfoil.
  - Each pressure tube was systematically connected to individual channels on the pressure scanner, ensuring organized and reliable mapping of pressure tap positions to scanner inputs.
  - The digital manometer had two ports:
    * One port was connected to the output of the pressure scanner.
    * The other port was left open to the atmosphere, allowing for gauge pressure measurement (i.e., pressure relative to ambient atmospheric pressure).
  - The pressure scanner allowed for channel selection via a digital interface. By selecting a channel on the scanner's display, *the corresponding pressure tap could be monitored*.
  - The digital manometer displayed the gauge pressure corresponding to the currently selected channel, enabling accurate and sequential recording of pressure values at all 20 tap locations.

Image: Pressure scanner

Image: Digital Manometer

Image: Pressure tubes connected to the pressure taps on the Airfoil

- **Wind Tunnel setup:**
  - The experiment was performed in a closed-circuit wind tunnel, allowing controlled and consistent airflow for aerodynamic testing.
  - Air velocity inside the tunnel could be adjusted by varying the fan frequency using a control meter. An increase in frequency resulted in a corresponding increase in airflow velocity across the Airfoil.
  - *To ensure consistency throughout the experiment*, the specific frequencies corresponding to desired velocities were noted and used during all measurements.
- **Pitot Tube and Velocity Measurement**
  - A Pitot-static tube was placed in the *test section of the wind tunnel* to measure airflow velocity.
  - The Pitot tube provided both *total pressure* and static pressure, with their difference indicating dynamic pressure.
  - This pressure difference was *measured* using a digital manometer, connected to the Pitot tube and *it gave us* the velocity for each wind speed setting.

Image of a pitot tube

Readings were taken for three different angles of attack (AoA), and for each AoA, the Airfoil was tested at three distinct wind speeds.

Final setup:

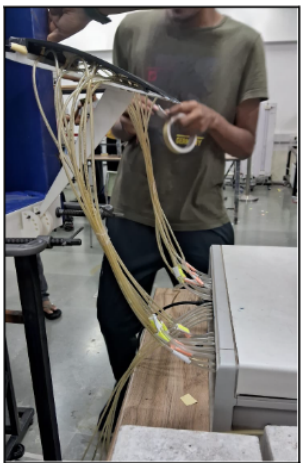
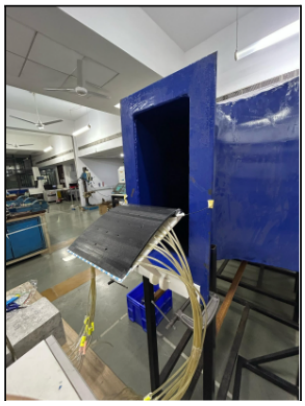
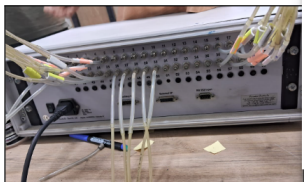

Schematic Diagram:

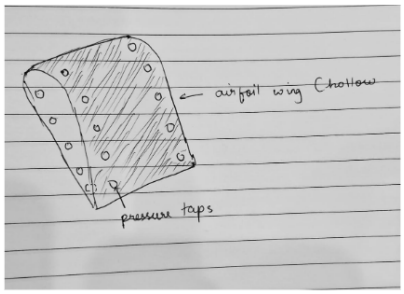

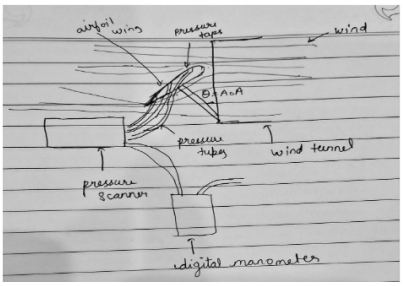

Pressure Tap Locations

We collected pressure readings from strategically drilled holes on the airfoil surface to begin the analysis. These were distributed symmetrically on the upper and lower surfaces, with five holes on the left side and five on the right side of the chord.

The figures below show the labelled airfoil geometry and tube mappings used during the experiments.

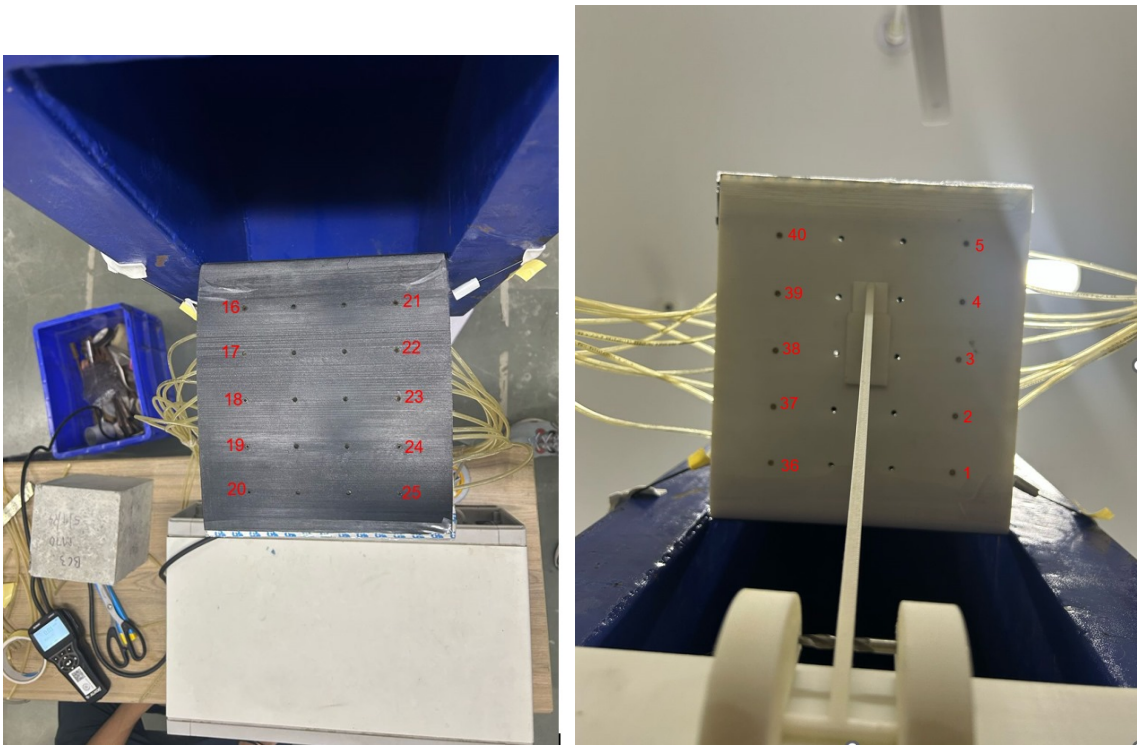

Figure 1: Labelled Airfoil with pressure tap tube numbers on upper and lower surfaces.

Measurements

These are the Dimensions of the Airfoil

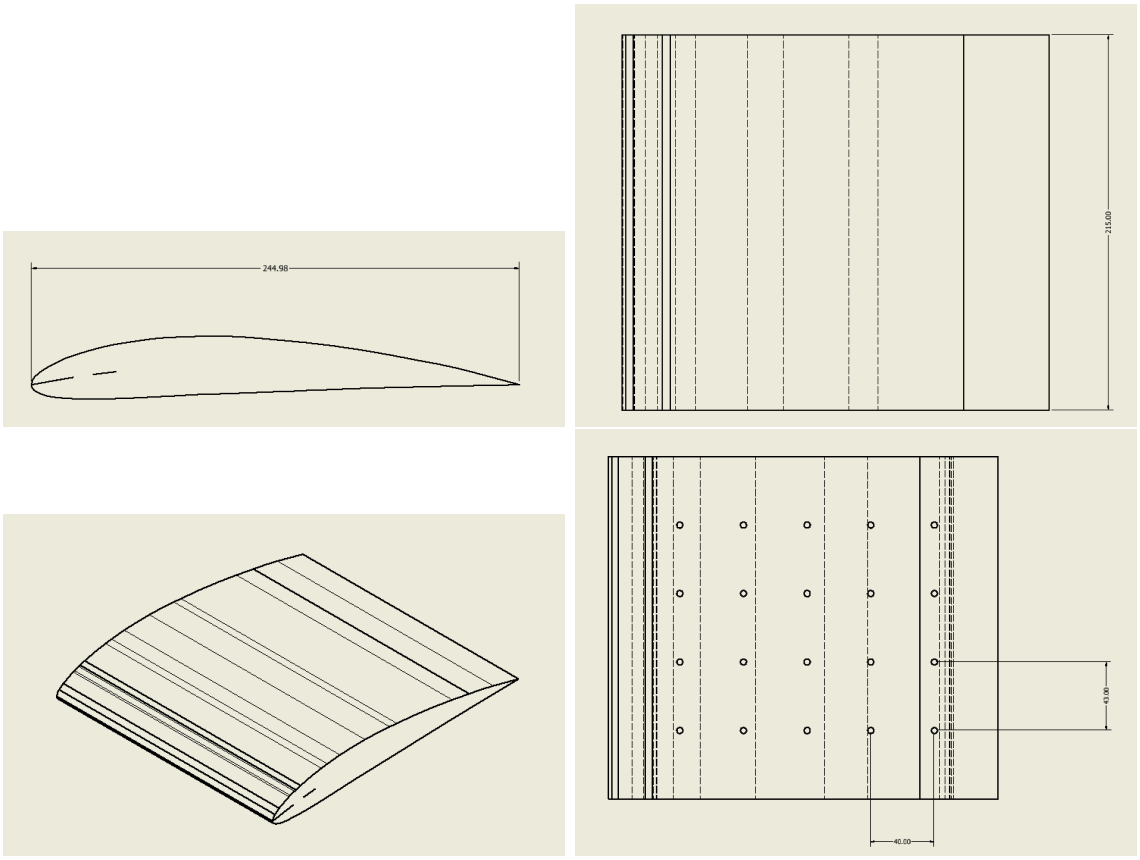

Figure 2: Horizontal Distance between the holes is 40 mm and vertical distance is 43 mm, width is 215 mm and Chord Length is 244.98 mm

Vertical distance between the holes on the lower and upper side of the Airfoil

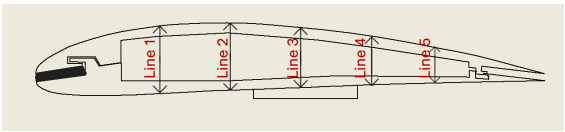

Figure 3: Vertical Distance in mm

- Line 1: 30.05 mm
- Line 2: 28.07 mm
- Line 3: 26.67 mm

- Line 4: 22.28 mm
- Line 5: 13.82 mm

Results

Lift Coefficient Estimation from Pressure Measurements

This experiment aims to determine an airfoil's aerodynamic performance by calculating its lift coefficient C_L using pressure distribution data collected over its surface. This section* explains the methodology and underlying theory in detail, from raw measurements to the final aerodynamic parameter.

1. Surface Pressure Measurement Setup

To analyse the pressure distribution over the Airfoil, a total of 20 pressure ports were drilled into the 3d-printed Airfoil at five discrete chordwise locations (denoted as $x_1, x_2, ..., x_5$). At each x_i, four ports were placed:

- Two on the right surface — one on the upper surface (ports 21–25) and one on the lower surface (ports 1–5),
- Two on the left surface — one on the upper surface (ports 16–20) and one on the lower surface (ports 36–40).

This symmetric arrangement allowed us to capture the spanwise pressure gradient and ensure that any local anomalies could be averaged. Each pressure reading was taken twice using a digital manometer (in mm H_2O), and the average of the two was recorded to reduce random noise.

2. Physical Basis: Pressure Difference as Source of Lift

From classical aerodynamics, the lift generated by an airfoil results from the pressure difference between the lower and upper surfaces. According to Bernoulli's principle, higher

velocity regions correspond to lower static pressure, and vice versa. As the angle of attack increases, the flow accelerates more over the upper surface, resulting in a pressure drop and thus a positive pressure difference $\Delta p = p_{\text{lower}} - p_{\text{upper}}$, which contributes to lift.

To compute this net pressure differential at each chordwise station, we used both sides of the Airfoil (left and right) to mitigate measurement asymmetry and hardware imperfections:

$$\Delta p_i = \frac{(p_{\text{lower}} - p_{\text{upper}})_{\text{right}} + (p_{\text{lower}} - p_{\text{upper}})_{\text{left}}}{2}$$

This symmetric averaging removes skewness due to local flow separation, instrument calibration errors, or structural asymmetries.

3. Unit Conversion and Scaling

The digital manometer reported pressure in mm of water column (mm H_2O), a commonly used unit in low-speed aerodynamic testing. To convert this into SI units (Pascals), we used the conversion:

$$1\,\text{mm } H_2O = 9.81\,\text{Pa}$$

This allowed consistent integration with dynamic pressure formulas and standardised aerodynamic coefficients.

4. Estimating Lift per Unit Span

The lift force per unit span, denoted as L' (in N/m), is the net vertical force acting on a vertical slice of the Airfoil of unit width. Since pressure acts normal to the surface, and the holes are symmetrically distributed across the chord (in vertical lines), the contribution from each pressure port pair can be modelled as vertical force components.

We approximate the total lift per unit span by integrating the pressure difference distribution over the chord of the Airfoil. Given discrete data points at x_1 to x_5, the trapezoidal integration method was used:

$$L' \approx \sum_{i=1}^{n-1} \frac{\Delta p_i + \Delta p_{i+1}}{2} \cdot (x_{i+1} - x_i)$$

Each term in the summation represents the net vertical force over a small chord segment Δx. The assumption here is that the pressure varies linearly between successive data points — a valid approximation given the high resolution of the pressure port locations.

5. Lift Coefficient Computation

To make the lift measurement comparable across different speeds, fluid densities, and airfoil sizes, we use the non-dimensional lift coefficient C_L, defined as:

$$C_L = \frac{L'}{\frac{1}{2}\rho U^2 c}$$

Where:

- L' is the lift per unit span (N/m),
- ρ is the air density (kg/m^3), typically estimated from the ambient temperature (e.g., 1.157 kg/m^3 at 32°C),
- U is the freestream velocity (m/s), measured via anemometer,
- c is the chord length of the Airfoil (in meters), obtained from CAD.

This final equation scales the raw force data with dynamic pressure and chord dimension, giving a universal metric that indicates the aerodynamic efficiency of the airfoil independent of test conditions.

6. Computation of Total Lift Force L from Lift per Unit Span L'

Once the pressure difference distribution across the chord of the Airfoil was obtained, the lift per unit span L' was calculated using the trapezoidal rule. This quantity represents the lift force generated per meter of spanwise length of the Airfoil.

However, to obtain the total lift force L exerted on the airfoil model, we must scale this value by the airfoil's physical span (or width) in the spanwise direction.

Formula Used:

$$L = L' \times b$$

Where:

- L is the total lift force (in Newtons),
- L' is the lift force per unit span (N/m),
- b is the span of the Airfoil (in meters).

This final lift value represents the net vertical force generated by the Airfoil due to the pressure difference between the upper and lower surfaces over the whole span.

Summary

We reconstructed the aerodynamic loading over the Airfoil's surface by drilling pressure ports and measuring static pressure differences along the airfoil chord. The differential pressure data was used to compute the distributed lift, which was then integrated to estimate the total lift force per unit span. Normalising with the dynamic pressure yielded the lift coefficient C_L, a fundamental parameter in evaluating airfoil performance at different angles of attack and freestream velocities.

Calculation of Lift Coefficient for AoA = 17.89° and Freestream Velocity = 8.175 m/s

readings:

Table 1: Pressure Readings for freq = 10.72 (vel = 8.175 m/s)

Surface	1	2	3	4	5	21	22	23	24	25
Right Trial 1	0.49	0.65	0.15	0.41	0.41	-2.23	-0.75	-0.35	-0.10	0.10
Right Trial 2	0.51	0.69	0.18	0.44	0.42	-2.19	-0.69	-0.20	-0.04	-0.02
Surface	16	17	18	19	20	36	37	38	39	40
Left Trial 1	-1.91	-0.5	-0.28	-0.06	-0.06	0.93	0.6	0.43	0.49	-0.06
Left Trial 2	-1.93	-0.71	-0.47	-0.25	-0.1	1.2	0.71	0.45	0.52	-0.02

Step 1: Extract and Average Pressure Readings (in mm H_2O)

Right Surface

Serial	**Readings**	**Average (mm H_2O)**
1	0.49, 0.51	0.500
2	0.65, 0.69	0.670
3	0.15, 0.18	0.165
4	0.41, 0.44	0.425
5	0.41, 0.42	0.415
21	-2.23, -2.19	-2.210
22	-0.75, -0.69	-0.720
23	-0.35, -0.20	-0.275
24	-0.10, -0.04	-0.070
25	0.10, -0.02	0.040

Left Surface

Serial	Readings	Average (mm H_2O)
16	-1.91, -1.93	-1.920
17	-0.50, -0.71	-0.605
18	-0.28, -0.47	-0.375
19	-0.06, -0.25	-0.155
20	-0.06, -0.10	-0.080
36	0.93, 1.20	1.065
37	0.60, 0.71	0.655
38	0.43, 0.45	0.440
39	0.49, 0.52	0.505
40	-0.06, -0.02	-0.040

Step 2: Calculate Δp (mm H_2O) = Lower - Upper

i	Right Lower - Upper	Left Lower - Upper
1	0.500 - (-2.210) = 2.710	1.065 - (-1.920) = 2.985
2	0.670 - (-0.720) = 1.390	0.655 - (-0.605) = 1.260
3	0.165 - (-0.275) = 0.440	0.440 - (-0.375) = 0.815
4	0.425 - (-0.070) = 0.495	0.505 - (-0.155) = 0.660
5	0.415 - 0.040 = 0.375	-0.040 - (-0.080) = 0.040

Step 3: Convert to Pascals (1 mm H_2O = 9.81 Pa)

i	Avg Δp_i (Pa)
1	$(2.710 + 2.985)/2 \times 9.81 = 26.89$ Pa
2	$(1.390 + 1.260)/2 \times 9.81 = 12.99$ Pa
3	$(0.440 + 0.815)/2 \times 9.81 = 6.17$ Pa
4	$(0.495 + 0.660)/2 \times 9.81 = 5.68$ Pa
5	$(0.375 + 0.040)/2 \times 9.81 = 2.03$ Pa

Step 4: Coordinates of Holes Along Chord (Assumed as before)

i	x_i (m)
1	0.04498
2	0.08498
3	0.12498
4	0.16498
5	0.20498

Step 5: Integration via Trapezoidal Rule

$$L' \approx \sum_{i=1}^{4} \frac{\Delta p_i + \Delta p_{i+1}}{2} \cdot (x_{i+1} - x_i)$$

$$\begin{aligned} L' = & \frac{26.89 + 12.99}{2} \cdot (0.08498 - 0.04498) \\ & + \frac{12.99 + 6.17}{2} \cdot (0.12498 - 0.08498) \\ & + \frac{6.17 + 5.68}{2} \cdot (0.16498 - 0.12498) \\ & + \frac{5.68 + 2.03}{2} \cdot (0.20498 - 0.16498) \\ & = 0.798 + 0.383 + 0.237 + 0.154 = \boxed{1.572 \text{ N/m}} \end{aligned}$$

Lift per unit span at AoA = 17.89° and $U_\infty = 8.17459$ m/s:

$$\boxed{L' \approx 1.572 \text{ N/m}}$$

Step 6: Lift Coefficient Calculation

To calculate the lift coefficient C_L, we use the formula:

$$C_L = \frac{L'}{\frac{1}{2}\rho U_\infty^2 c}$$

Where:

- $L' = 1.572$ N/m (from previous calculation)
- $\rho = 1.225$ kg/m^3 (air at sea level)
- $U_\infty = 8.17459$ m/s
- $c = 0.25$ m (chord length)

$$\begin{aligned}\frac{1}{2}\rho U_\infty^2 c &= \frac{1}{2} \cdot 1.225 \cdot (8.17459)^2 \cdot 0.25 \\ &= 0.5 \cdot 1.225 \cdot 66.8259 \cdot 0.25 \approx 10.229 \text{ N/m} \\ C_L &= \frac{1.572}{10.229} \approx \boxed{0.154}\end{aligned}$$

Step 7: Computation of Total Lift Force L

From the trapezoidal integration, we previously found the lift per unit span as:

$$L' = 1.572\,\text{N/m}$$

Given the span of the airfoil model:

$$b = 0.215\,\text{m}$$

Then, the total lift is:

$$L = L' \times b = 1.572 \times 0.215 = \boxed{0.3380\,\text{N}}$$

Final Answer: Lift Coefficient $C_L \approx 0.154$ and Lift Force $L = 0.3380$ N at AoA $= 17.89°$, $U_\infty = 8.17459$ m/s.

Pressure Readings with their Final Lift Coefficients for each case

The following tables present all raw pressure readings obtained using a digital manometer at various flow velocities and angles of attack. Each reading is recorded in mm H_2O, and two iterations were taken for each hole to ensure reliability.

Angle of Attack = 0°

Raw Pressure Readings (unit: mm H_2O)

Table 2: Pressure Readings for freq = 8.4 (vel = 6.4 m/s)

Surface	1	2	3	4	5	21	22	23	24	25	
Right Trial 1	-0.26	0.15	-0.08	0.10	0.11	-0.70	-0.46	-0.15	0.03	-0.01	
Right Trial 2	-0.26	0.14	-0.08	0.09	0.11	-0.73	-0.47	-0.17	0.02	0.00	
Surface	16	17	18	19	20	36	37	38	39	40	
Left Trial 1	-0.72	-0.42	-0.23	-0.05	-0.04	-0.11	0.07	0.03	0.08	0.04	
Left Trial 2	-0.72	-0.43	-0.22	-0.04	-0.04	-0.1	0.08	0.03	0.08	0.04	

Table 3: Pressure Readings for freq = 10.72 (vel = 8.175 m/s)

Surface	1	2	3	4	5	21	22	23	24	25
Right Trial 1	-0.40	0.18	-0.13	0.12	0.08	-1.08	-0.68	-0.16	0.01	-0.05
Right Trial 2	-0.45	0.08	-0.19	0.10	0.14	-1.27	-0.86	-0.34	0.02	-0.02
Surface	16	17	18	19	20	36	37	38	39	40
Left Trial 1	-1.12	-0.60	-0.34	-0.04	-0.05	-0.2	0.09	0.01	0.09	-0.14
Left Trial 2	-1.20	-0.67	-0.43	-0.08	-0.12	-0.18	0.11	0.01	0.11	-0.15

Table 4: Pressure Readings for freq = 13.6 (vel = 10.45 m/s)

Surface	1	2	3	4	5	21	22	23	24	25
Right Trial 1	-0.46	0.22	-0.33	0.02	-0.03	-1.61	-0.78	-0.31	-0.21	-0.11
Right Trial 2	-0.44	0.23	-0.32	0.03	-0.02	-1.60	-0.77	-0.30	-0.20	-0.10
Surface	16	17	18	19	20	36	37	38	39	40
Left Trial 1	-1.86	-0.92	-0.64	-0.17	-0.22	-0.44	0.04	-0.21	0.27	-1.05
Left Trial 2	-1.85	-0.91	-0.63	-0.16	-0.21	-0.43	0.05	-0.2	0.28	-1.04

Final Results for Angle of Attack = 0°

Table 5: Summary of Lift Force and Coefficient for Various Freestream Velocities

Freestream Velocity (m/s)	L' **(N/m)**	C_L	L **(N)**
6.41	0.619	0.106	0.133
8.175	0.952	0.101	0.2057
10.45	1.395	0.09	0.2999

Angle of Attack = 17.89°

Raw Pressure Readings (unit: mm H_2O)

Table 6: Pressure Readings for freq = 8.4 (vel = 6.4 m/s)

Surface	1	2	3	4	5	21	22	23	24	25
Right Trial 1	0.43	0.45	0.18	0.3	0.28	-1.38	-0.42	-0.22	-0.07	-0.06
Right Trial 2	0.4	0.47	0.21	0.31	0.29	-1.38	-0.44	-0.2	-0.02	-0.05
Surface	16	17	18	19	20	36	37	38	39	40
left Trial 1	-1.21	-0.29	-0.19	-0.1	-0.03	0.56	0.36	0.25	0.29	0.01
left Trial 2	-1.19	-0.28	-0.18	-0.02	-0.03	0.57	0.39	0.29	0.31	-0.01

Table 7: Pressure Readings for freq = 10.72 (vel = 8.175 m/s)

Surface	1	2	3	4	5	21	22	23	24	25
Right Trial 1	0.49	0.65	0.15	0.41	0.41	-2.23	-0.75	-0.35	-0.10	0.10
Right Trial 2	0.51	0.69	0.18	0.44	0.42	-2.19	-0.69	-0.20	-0.04	-0.02
Surface	16	17	18	19	20	36	37	38	39	40
Left Trial 1	-1.91	-0.5	-0.28	-0.06	-0.06	0.93	0.6	0.43	0.49	-0.06
Left Trial 2	-1.93	-0.71	-0.47	-0.25	-0.1	1.2	0.71	0.45	0.52	-0.02

Table 8: Pressure Readings for freq = 13.6 (vel = 10.45 m/s)

Surface	1	2	3	4	5	21	22	23	24	25
Right Trial 1	1.11	1.19	0.35	0.77	0.70	-2.75	-1.35	-0.67	-0.21	-0.18
Right Trial 2	1.11	1.19	0.34	0.78	0.73	-2.75	-1.35	-0.66	-0.20	-0.18
Surface	16	17	18	19	20	36	37	38	39	40
Left Trial 1	-2.56	-1.06	-0.65	-0.22	-0.16	1.65	0.98	0.7	0.8	-0.2
Left Trial 2	-2.55	-1.02	-0.65	-0.22	-0.21	1.67	0.99	0.69	0.8	-0.2

Final Results for Angle of Attack = 17.89°

Table 9: Summary of Lift Force and Coefficient for Various Freestream Velocities

Freestream Velocity (m/s)	L' **(N/m)**	C_L	L **(N)**
6.41	0.998	0.172	0.2146
8.175	1.572	0.154	0.3370
10.45	2.629	0.1571	0.5652

Angle of Attack = 35.78°

Raw Pressure Readings (unit: mm H_2O)

Table 10: Pressure Readings for freq = 8.4 (vel = 6.4 m/s)

Surface	1	2	3	4	5	21	22	23	24	25
Right Trial 1	0.85	0.78	0.44	0.53	0.38	-0.93	-1.04	-0.74	-0.64	-0.65
Right Trial 2	0.87	0.79	0.45	0.53	0.38	-0.99	-1.02	-0.77	-0.62	-0.68
Surface	16	17	18	19	20	36	37	38	39	40
Left Trial 1	-1.00	-0.87	-1.00	-0.64	-0.43	1.12	0.74	0.58	0.52	0.06
Left Trial 2	-0.95	-0.88	-1.02	-0.65	-0.39	1.12	0.75	0.59	0.53	0.06

Table 11: Pressure Readings for freq = 10.72 (vel = 8.175 m/s)

Surface	1	2	3	4	5	21	22	23	24	25
Right Trial 1	1.39	1.27	0.66	0.84	0.62	-1.73	-1.73	-1.29	-1.38	-1.03
Right Trial 2	1.41	1.28	0.68	0.84	0.60	-1.73	-1.74	-1.26	-1.37	-1.06
Surface	16	17	18	19	20	36	37	38	39	40
Left Trial 1	-1.56	-1.52	-1.66	-1.10	-0.66	1.81	1.18	0.93	0.84	0.03
Left Trial 2	-1.65	-1.50	-1.74	-1.08	-0.64	1.83	1.21	0.95	0.85	0.02

Table 12: Pressure Readings for freq = 13.6 (vel = 10.45 m/s)

Surface	1	2	3	4	5	21	22	23	24	25
Right Trial 1	2.13	1.88	0.88	1.24	0.91	-2.84	-2.74	-2.40	-2.36	-1.66
Right Trial 2	2.18	1.93	0.90	1.25	0.93	-2.96	-2.78	-2.59	-2.45	-1.58
Surface	16	17	18	19	20	36	37	38	39	40
Left Trial 1	-3.04	-2.73	-2.82	-1.42	-0.68	2.79	1.78	1.4	1.31	-0.06
Left Trial 2	-3.28	-2.85	-2.93	-1.42	-0.73	2.88	1.87	1.48	1.37	-0.07

Final Results for Angle of Attack = 35.78°

Table 13: Summary of Lift Force and Coefficient for Various Freestream Velocities

Freestream Velocity (m/s)	L' **(N/m)**	C_L	L **(N)**
6.41	2.415	0.415	0.5192
8.175	4.075	0.430	0.8759
10.45	6.637	0.429	1.4279

Reynolds Number Calculations

The Reynolds number Re is a dimensionless quantity that characterises the flow regime of a fluid. It is defined as:

$$Re = \frac{\rho U_\infty c}{\mu}$$

Where:

- $\rho = 1.157\,\mathrm{kg/m^3}$ is the density of air at room temperature,
- U_∞ is the freestream velocity in m/s,
- $c = 0.24498\,\mathrm{m}$ is the chord length of the airfoil,
- $\mu = 1.85 \times 10^{-5}\,\mathrm{Pa \cdot s}$ is the dynamic viscosity of air.

Using this formula, we calculate the Reynolds number for each case:

For $U_\infty = 6.41\,\mathbf{m/s}$:

$$Re = \frac{1.157 \times 6.41 \times 0.24498}{1.85 \times 10^{-5}} = \frac{1.813}{1.85 \times 10^{-5}} \approx \boxed{9.8 \times 10^4}$$

For $U_\infty = 8.175\,\mathbf{m/s}$:

$$Re = \frac{1.157 \times 8.175 \times 0.24498}{1.85 \times 10^{-5}} = \frac{2.317}{1.85 \times 10^{-5}} \approx \boxed{1.25 \times 10^5}$$

For $U_\infty = 10.45\,\mathbf{m/s}$:

$$Re = \frac{1.157 \times 10.45 \times 0.24498}{1.85 \times 10^{-5}} = \frac{2.964}{1.85 \times 10^{-5}} \approx \boxed{1.60 \times 10^5}$$

Uncertainty analysis

This experiment measured the aerodynamic lift characteristics of a cambered airfoil (confirmed to match NACA 4412 geometry) at three angles of attack (α): 0°, 17.89°, and 35.78°. Freestream velocities (U_∞) were varied as 6.41 m/s, 8.175 m/s, and 10.45 m/s. Lift per unit span (L') was computed using interpolated pressure differences between the upper and lower surfaces (5 points each). Total lift force (L) was obtained by multiplying L' with the span (0.215 m). Lift coefficients (C_L) were calculated using:

$$C_L = \frac{L'}{\frac{1}{2}\rho U_\infty^2 c}$$

Table 14: Measured Lift per Unit Span, Lift Force(L), and Lift Coefficient

Angle of Attack	U_∞ **(m/s)**	L' (N/m)	L (N)	C_L
0°	6.41	0.619	0.133	0.106
	8.175	0.952	0.205	0.101
	10.45	1.395	0.300	0.090
17.89°	6.41	0.998	0.215	0.172
	8.175	1.572	0.338	0.154
	10.45	2.629	0.565	0.157
35.78°	6.41	2.415	0.519	0.415
	8.175	4.075	0.876	0.430
	10.45	6.637	1.427	0.429

Key Observations

- For each fixed α,Lift force increases with increase in U_∞, as expected from lift's quadratic dependence on velocity.
- Even at $\alpha = 0°$, the Airfoil produces lift, consistent with cambered airfoils like NACA 4412 which are known to have positive C_L at zero incidence.

- At higher angles (notably $\alpha = 35.78°$), C_L continues to rise, suggesting that stall has not yet occurred—unusual for most conventional airfoils.

Comparison with Literature

We compare the experimental results with standard curves from the literature for similar Reynolds numbers to validate them.

- **NACA 4412:** Literature reports $C_L@0° \approx 0.25$ and a slope of about 0.11 per degree up to stall (at $\sim$15°). Our C_L at 0° is significantly lower ($\sim$0.1), but the overall trend of increasing C_L with α is preserved.

Reasons for Differences from Literature

Despite geometric similarity to NACA 4412, the experimental results deviate notably in terms of lift magnitude and stall characteristics. Possible reasons include:

1. **Low Reynolds Number Effects:** The Reynolds number in the experiment is estimated to be in the range of 10^5 to 1.6×10^5, which is much lower than the typical values ($\sim 10^6$) for standard NACA data. At low Re, the boundary layer is more susceptible to laminar separation, and flow reattachment behaviour can differ significantly, delaying stall or reducing C_L.
2. **Surface Finish and Boundary Layer Transition:** In professional tests, a rough strip (trip) is added to make the flow turbulent at a known location. This wasn't done in our test, so the airflow transition may have happened differently, affecting lift and stall behaviour.
3. **Pressure Tap Limitation:** In our experiment, we used 20 pressure taps — 5 on the upper surface and five on the lower surface of the Airfoil, placed on both sides. These taps were distributed from the leading edge to the trailing edge, allowing us to estimate the pressure difference across the chord. The pressure distribution over an airfoil can change sharply near the leading edge, especially at high angles of attack. Stall or flow separation can start in a localised region, which may fall between two taps and go undetected. With more taps (e.g., 10+ per surface), the resolution of the

pressure profile would improve, especially in capturing subtle flow features like early separation or peak suction.

4. **Experimental Uncertainty:** While specific numerical uncertainties were not quantified, possible sources include calibration of sensors, resolution of interpolation, alignment errors in angle setting, and unsteady inflow.

Uncertainty Considerations

Though numerical uncertainty analysis was not feasible due to unavailable $\delta L'$, δU, and δc, qualitative uncertainties can still be discussed:

- **Measurement Repeatability:** Lift values were inferred from interpolated pressure readings. Minor errors in reading pressure taps or sensor drift could affect values.
- **Angle Setting Accuracy:** The actual anAnglef attack may slightly deviate from the set value due to manual mounting or scale error.
- **Spatial Resolution:** Only five pressure difference readings per surface limit pressure distribution and lift integration fidelity.
- **Methodological Assumptions:** The standard method assumes pressure forces act vertically on both surfaces, but this is an approximation. An alternate method considers the direction of pressure forces more accurately, as explained below.

Alternate Lift Calculation Method

While the primary method for estimating lift involved taking pressure differences between corresponding upper and lower surface taps, a more physically accurate approach considers the direction of the pressure forces and their vertical components.

Pressure Force Direction

The pressure force at any point on the Airfoil acts normal (perpendicular) to the local surface. This direction varies along the Airfoil:

- On the **lower surface**, the Airfoil is relatively flat or gently curved. Thus, the pressure force direction is nearly vertical, closely aligned with the lift direction.
- On the **upper surface**, the surface is more curved. Here, the pressure force still acts normal to the local surface, but that normal vector is tilted away from vertical. Hence, only a component of this force contributes to lift.

Component Resolution for Lift

Lift acts vertically, perpendicular to the freestream in our setup. Therefore, we cannot directly sum all pressure forces. Instead, for each tap:

- Determine the angle θ_i between the surface normal and the vertical direction at that tap location.
- Compute only the **vertical component** of the local pressure force:

$$F_{y,i} = P_i \cdot A_i \cdot \cos(\theta_i)$$

  Where:

  - P_i is the local gauge pressure at tap i,
  - A_i is the surface area represented by tap i,
  - θ_i is the angle between the surface normal and vertical.

Local Area Contribution

Each pressure tap corresponds to a segment of the Airfoil:

- Spanning a certain length in the chordwise direction (between adjacent taps),
- And a fixed spanwise width (equal to the wind tunnel width or effective airfoil span).

The total lift is obtained by summing the vertical components of pressure forces from all taps on both surfaces:

$$L = \sum_{i \in \text{lower}} P_i \cdot A_i + \sum_{j \in \text{upper}} P_j \cdot A_j \cdot \cos(\theta_j)$$

This approach improves accuracy by properly resolving force direction, especially critical at high angles of attack where curvature and flow separation are more pronounced.

References

- Anderson, J. D. (2017). *Fundamentals of Aerodynamics* (6th ed.). McGraw-Hill Education.
- Çengel, Y. A., & Cimbala, J. M. (2018). *Fluid Mechanics: Fundamentals and Applications* (4th ed.). McGraw-Hill Education.
- White, F. M. (2011). *Fluid Mechanics* (7th ed.). McGraw-Hill Education.

Conclusion

This experiment explored the lift characteristics of a cambered airfoil (NACA 4412) at various wind speeds and angles of attack. We calculated the lift force and the corresponding lift coefficient (CL) under different flow conditions by measuring surface pressures. As expected, lift increased with both freestream velocity and an angle of attack. Interestingly, the Airfoil produced positive lift even at 0°, confirming the cambered airfoils' behaviour. At higher angles like 35.78°, the CL continued to rise without signs of stall, which is unusual and likely due to our setup's low Reynolds numbers and laminar flow conditions. These findings highlighted how experimental conditions such as surface finish, pressure tap resolution, and Reynolds number can significantly affect aerodynamic performance. The experiment successfully fulfilled its primary objective of measuring lift forces at different angles of attack. It also gave us meaningful hands-on experience in aerodynamic testing and data analysis. Through this process, we better understood the relationship between pressure distribution and lift generation. We learned the importance of experimental design and uncertainty analysis in fluid dynamics studies.

Acknowledgement:

We would like to express our sincere gratitude to IIT Gandhinagar for offering the course ME207: Fluid Dynamics, which has allowed us to learn and practically apply several fundamental concepts of fluid dynamics.

We extend our heartfelt thanks to Prof. Dilip Srinivas Sundaram for his invaluable instruction in the theoretical aspects of the course and to Prof. Uddipta Ghosh for designing the laboratory experiments, which allowed us to engage with various practical setups.

Lastly, we sincerely appreciate the guidance and support of the teaching assistants for clarifying doubts and helping us whenever we encountered challenges during the lab.